JOURNAL OF MATERIALS SCIENCE 21 (1986) 810–824

Creep and fracture of a vitreous-bonded aluminium oxide

S. M. WIEDERHORN, B. J. HOCKEY, R. F. KRAUSE, Jr
National Bureau of Standards, Gaithersburg, Maryland 20899, USA

K. JAKUS
University of Massachusetts, Amherst, Massachusetts 01003, USA

Creep and creep-rupture behaviour of a commercial grade of glass-bonded, 96% aluminum oxide was characterized as a function of temperature and applied stress. The creep data were fitted to the classical empirical relation usually used to describe this phenomenon. The apparent activation enthalpy, $\Delta H = 926\,\text{kJ mol}^{-1}$, and the stress exponent, $n = 4.8$, lie at the high end of the range reported for two-phase materials, primarily as a result of structural modifications that occur during creep. A stress-modified Monkman–Grant relationship was fitted to the creep-rupture data to give a stress exponent of -4.2. None of the available theories of creep rupture provided a satisfactory description of the present set of data. Analytical electron microscopy was used to characterize the composition and structure of this material. In the as-received material the intergranular phase was a glass of nearly uniform composition. During high-temperature exposure, devitrification of the glass resulted in the formation of various crystalline phases within the intergranular region of the material. Devitrification depended on both the proximity to the surface, where it was most pronounced, and on the state of stress. In this regard, flexural creep samples exhibited extensive crystallization within the tensile region of the flexural specimens, but little crystallization within the compressive cross-section. From the composition of the retained glass, estimates of the viscosity of the glass at the grain boundaries were made and used, in combination with microstructural information, to compare the creep behaviour with available theories of creep. The results of this paper are consistent with percolation and solution precipitation mechanisms of creep deformation. By contrast, cavitation did not seem to play a major role in the creep deformation process.

1. Introduction

Current interest in the mechanical behaviour of multiphase ceramics has its origin in the potential use of these materials in high-temperature structural applications. In the automotive industry, for example, two-phase ceramics such as sintered silicon nitride and glass-bonded cordierite are being used as structural materials for combustors, turbines, turbochargers and heat regenerators [1]. In the power industry, two-phase materials are being considered for heat recouperators and for linings in slagging gasifiers [2]. In these applications, the mechanical response of the ceramic to external forces depends on the microstructure, in particular on the refractoriness and chemical activity of the phases that make up the ceramic. Most high-temperature structural ceramics consist of highly refractory grains bonded by a less refractory vitreous intergranular phase. Therefore, creep and creep rupture of these materials depend primarily on the physical and chemical properties of the vitreous phase and on the amount and distribution of the vitreous phase within the ceramic structure.

Because of the importance of the intergranular vitreous phase for the structural integrity of high-temperature ceramics, most recent studies on these materials have concentrated on characterizing the behaviour of the vitreous phase as a means of understanding the behaviour of the ceramic composite. Thus, Lange *et al.* [3] have shown how the compressive creep behaviour of silicon nitride can be modified by changing the composition and volume fraction of the glassy phase within hot-pressed silicon nitride. These authors also demonstrated that high-temperature exposure, which removes glass modifiers from the vitreous matrix, also greatly reduces the susceptibility of the hot-pressed silicon nitride to creep [4]. These findings reinforced earlier findings of Kossowsky, Miller and Diaz [5], who showed that glass modifiers, such as calcium, reduce the viscosity of glass and therefore increase the susceptibility of hot-pressed silicon nitride to creep. Similar findings were made by others on porcelains [6], fire bricks [7] and glass ceramics [8].

Despite our general understanding of the importance of glass composition and structure in creep and fracture, it is only now with the development of high resolution analytical microscopy that the chemical composition of the glass bonding phase can be deter-

0022–2461/86 $03.00 + .12

mined. Evaluation of the glass composition opens the possibility of estimating physical properties of the glass matrix, such as diffusivity or viscosity, which are required for the critical evaluation of most theories of creep and creep rupture. By analysing the composition of the vitreous matrix, these physical properties can either be determined experimentally on a similar composition of glass, or estimated theoretically, and a direct comparison between these theories of creep and creep rupture, and experimental creep and creep-rupture data, can then be made.

In this paper analytical electron microscopy is used to elucidate the creep and creep-rupture behaviour of a commercial grade of vitreous bonded aluminum oxide. The chemical composition of the glass bonding phase is determined before and after static annealing and creep deformation. From the chemical compositions, theoretical estimates of the viscosity of the glasses are made in order to compare creep and creep-rupture theory with experimental data. The electron microscope is also used in a more classical way: as a method of identifying changes in the microstructure that occur during creep. Using these methods, the creep rate is shown to be determined by the viscosity of the glass, suggesting that viscous flow and/or solution precipitation contribute to the creep process. Although cavitation is not observed to occur homogeneously in our specimens, cavitation at select boundaries followed by crack growth is believed to be important in later stages of the creep process.

2. Experimental procedure

Creep and creep-rupture experiments were conducted on a commercial grade of vitreous bonded aluminum oxide, COORS AD–96,* reported to contain 96% aluminum oxide. Experiments were conducted using four-point bending as a test technique. This technique was selected for ease of testing and for the fact that specimens for the electron microscope could be obtained from the tensile and compressive portions of the same specimen, thus excluding thermal history and extent of strain in comparative analysis. Creep-test specimens, 3 mm high and 5 mm wide, were loaded on a bending fixture of silicon carbide with outer and inner loading points of 40 and 10 mm, respectively. Approximately half the specimens were polished on the tensile surface to permit identification of incipient failure sites and crack nuclei as they formed during creep. Dead-weight loads from 40 to 100 N were applied via a lubricated rubber diaphragm air cylinder, which, in combination with a two-step, continuous leak pressure regulator, was capable of maintaining the applied load to within ± 1.5 N. Stress and strain were calculated by the procedure given by Hollenberg *et al.* [9], assuming a stress exponent of unity. No further corrections to the estimated stresses and strains were made in the present paper.

The loading point displacement during creep was monitored by a linear voltage displacement transducer (LVDT) that was attached to the upper ram of the test equipment. The loading point displacement of specimens was measured to within $\pm 2\,\mu$m. To enhance the long-term accuracy of the displacement readings, a block of sintered silicon carbide, of the same grade as that used for the rams, was used in one of the three test stations in each furnace. Since the block did not undergo creep at the loads and temperatures used in the present study, any displacement measured by the LDVT on the block reflected changes in the test facility due to electronic drift or to fluctuations in the ambient temperature. These displacement fluctuations were subtracted from the displacements measured on the specimens in the other two stations of the same furnace, so as to minimize errors due to electronic drift or to differential thermal expansion of the test fixture. Even though two specimens were tested in the same furnace for each run, the failure of one specimen was never observed to affect the other in the course of our investigation, primarily because pneumatic pistons and rubber shock absorbers were used to restrain the propagation of stress waves.†

Recognizing that phase changes often occur in ceramics during extended high-temperature exposure [6, 7], most specimens were annealed at 1050° C for a period of 96 h before testing to stabilize the ceramic against composition or structural changes that might influence the creep behaviour. Since most of the creep studies in this programme were typically less than 100 h duration, it was hoped that this annealing period would be sufficient to ensure a constant structure for the present investigation. Despite this precaution, some phase changes were observed during creep. The affect of annealing on both creep and microstructure represents an important aspect of our results, and accordingly will be discussed extensively below.

To establish the temperature range to be investigated, a stepped-temperature creep test [10] was conducted using an initial applied stress of 60 MPa, which was approximately one-third of the reported breaking stress at 1000° C. In this test a constant load was applied to the specimen, and the temperature was increased at various time intervals either until failure occurred, or deformation was so severe that further creep was pointless. Significant creep activity for this material starts at approximately 950° C; at 1050° C the creep of the ceramic is relatively rapid, failure occurring in approximatey 24 h at approximately 0.14% strain. Based on these results, experiments were conducted at temperatures ranging from 980 to 1100° C, and at applied stresses ranging from 40 to 100 MPa.

Specimens for examination by transmission electron microscopy (TEM) were obtained from the deformed bend bars using standard sectioning, polishing and ion-milling techniques. Two types of sections were used in these studies (Fig. 1). Specimens with the major plane of the foil parallel to the plane of maximum tensile or compressive stress were used to analyse the near-surface regions of the specimen, i.e.

*Coors Porcelain Co., 600 Ninth Street, Golden, Colorado. Identification of this material is not to be construed as endorsement by the National Bureau of Standards.

†Bellows are a non-inertial method of loading the specimens, and the air gaps in the bellows do not permit the passage of a stress wave. Hence, when a specimen breaks, the stress waves resulting from the fracture are largely dissipated before reaching the second specimen.

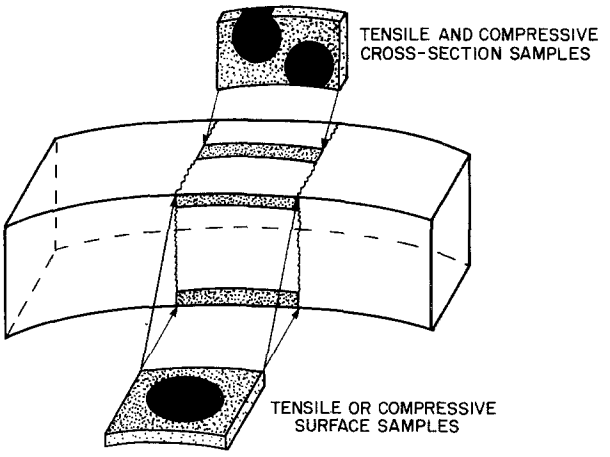

Figure 1 Schematic diagram of bend bar showing regions from which thin sections were prepared for examination by transmission electron microscopy.

from 0 to 50 μm from the external surface. Specimens with the plane of the foil perpendicular to the bending axes were used to examine changes in composition and structure at greater distances (0.2 to 1 mm) from the tensile or compressive surfaces of the creep specimens. This orientation was selected to examine the ceramic structure as a function of distance from the tensile and compressive surfaces of the bend bars.

3. Experimental results

3.1. Microstructure

A representative view of the material used in this study is shown in Fig. 2. The material consists principally of aluminum oxide grains (A) bonded by an intergranular glassy phase (M). Interspersed throughout the material there are also abnormally large grains of spinel ($MgAl_2O_4$), S, ranging in size from 20 to 40 μm, and irregularly shaped pores of microscopic (5 to 10 μm) dimensions. Using the line-intercept method, the mean grain size of Al_2O_3 was determined to be 8 μm, but ranged from 3 to 20 μm. The volume fraction of intergranular glassy phase, which was located primarily at multi-grain junctions, was roughly 8%. The porosity of the material was also roughly 8% by volume.

In applying TEM, major emphasis was placed on determining the structure and chemical composition of the intergranular phase. Chemical compositions were determined by energy dispersive X-ray analysis (EDX) using the ratio method in the thin-foil approximation [11] after background subtraction by linear extrapolation. The required K values for the various oxides‡ were determined from spectra obtained from two glass standards (Table I), which were also prepared by ion milling. In all cases, spectra from either the standards or the unknowns were taken under similar conditions (beam current, beam size, angle of tilt, etc.), a precaution necessitated by the presence of sodium in both the glass bonding phase and in one of the crystalline products of devitrification. The highly volatile nature of sodium during electron irradiation, moreover, placed severe restrictions on the imposed electron beam flux and duration of exposure. Most generally, this precluded the use of a focused probe regardless of other operating conditions and required the use of defocused beams of (typically) 400 μm or greater in diameter. While many grain-boundary widths were considerably smaller than this limiting probe size, most joined continuously with triple junctions of larger dimensions. As a check on spacial resolution, "hole count" spectra obtained from etched-out grain boundaries and triple junctions showed only an insignificant aluminum intensity enhancement, while differences in the elemental composition of the various intergranular phases allowed for a ready check on possible "overlap". In all cases, chemical compositions are given in terms of average values obtained from at least ten determinations.

Transmission electron microscopy provided not only a more detailed view of the microstructure, but also revealed that pronounced changes occur within the intergranular bonding phase due to prolonged static annealing and creep. In the as-received material, the intergranular bonding phase was found to consist entirely of a glass (Fig. 3). EDX analyses of the glass found at triple junctions (Fig. 3a), two-grain boundaries (Fig. 3b), and larger multi-grain junctions or "pockets" gave a fairly uniform composition listed in Table II. Though not particularly evident in Fig. 3, most Al_2O_3 grains were separated by a glass film

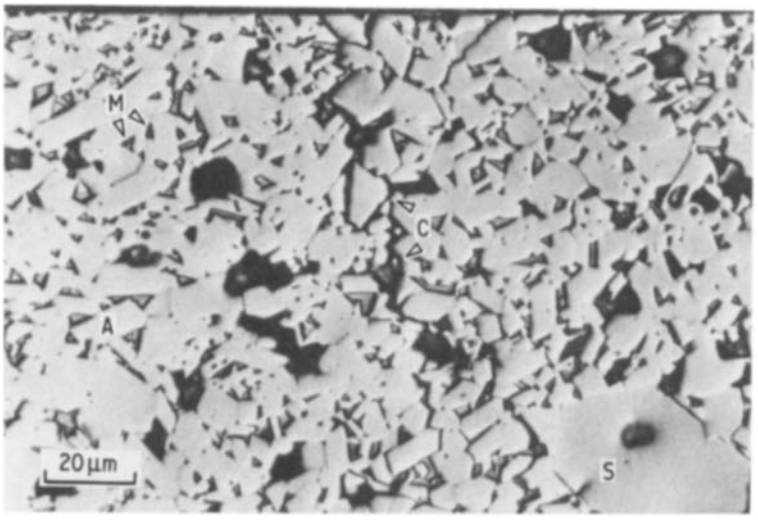

Figure 2 Light micrograph of longitudinal cross-section from creep sample. Relief polishing distinguishes intergranular phase (M) from aluminium oxide grains (A) and abnormally large spinel grains (S). Also evident are large pores, inherent in the material. Arrow indicates tensile creep crack that extends part way through the sample. Note that crack path is entirely intergranular.

‡It was assumed that all constituents were present as stoichiometric oxides.

TABLE I Glasses used for calibration purposes in the present study

Glass	Component (wt fraction)							
	SiO_2	Al_2O_3	B_2O_3	FeO	Na_2O	K_2O	MgO	CaO
Soda–lime silica	0.72	0.02	–	–	0.14	0.01	0.04	0.07
K–412*	0.45	0.09	–	0.10	–	–	0.19	0.15
C1720†	0.62	0.17	0.05	–	0.01	–	0.07	0.08
C0080†	0.73	0.01	–	–	0.17	–	0.04	0.05

*NBS Standard Reference Material, SRM 470. Compositions in the standard are reported to better than two significant figures.
†Corning Glass Co. See Hutchins and Harrington [21] for compositions. The use of this glass does not imply endorsement by the National Bureau of Standards.

which, due to the irregular morphology of the Al_2O_3 grains, ranged in thickness from roughly 10 nm upwards of several tenths of a micrometre. In this regard, the relatively wide, glassy grain-boundary region – as well as the apparent Al_2O_3 surface faceting – seen in Fig. 3b was not uncommon. The results thus indicate that, in the as-received condition, the bonding phase can be regarded as a continuously linked, glassy structure.

Upon prolonged annealing (1050° C, 96 h), pronounced changes were found within the bonding phase due to partial devitrification of the glass. Specifically, devitrification results in the formation of various crystalline phases and, as a consequence, changes the volume fraction and composition of the retained glassy phase. Although devitrification occurs throughout the samples, it is most pronounced within the surface regions. Accordingly, results obtained from the interior and from the surface regions of bulk, annealed samples are described separately. Within the interior of annealed samples, analytical electron microscopy revealed only the presence of two different magnesia aluminosilicate phases within the bonding phase: one having an average composition of $4MgO \cdot Al_2O_3 \cdot 4SiO_2$ and being isomorphic with orthorhombic enstatite ($MgSiO_3$), the other having an average composition of $2MgO \cdot 2Al_2O_3 \cdot SiO_2$ and being isomorphic with monoclinic sapphirine ($4MgO \cdot 5Al_2O_3 \cdot 2SiO_2$). Moreover, small crystallites of one or both of these phases were found within many, but not all, of the larger triple junctions or multi-grain "pockets" (Fig. 4a), and never within two-grain boundaries. Because of this, devitrification results in only a minor decrease in the volume fraction of the glassy phase, (estimated at less than 10%). This, however, is sufficient to produce a significant change in glass composition which from Table II is seen to be nearly depleted in MgO. Here it is important to note that the observed change in glass composition was uniform throughout the interior of annealed samples, regardless of whether localized crystallization had occurred.

As indicated earlier, devitrification was especially pronounced within the surface regions, where it is estimated that from 50 to 75% of the intergranular glassy phase devitrified during annealing. Although enhanced formation of both magnesio-aluminosilicate crystalline phases at the surface played a role in reducing the volume fraction of glass, the reduction of the glass fraction was primarily related to the formation of a triclinic, sodium–calcium aluminosilicate phase identified by electron diffraction and chemical analyses (Table II) as intermedite plagioclase.§ Unlike the magnesio-aluminosilicate phases, the intermedite plagioclase formed more uniformly throughout the intergranular regions and often resulted in the (apparently) complete crystallization of two-grain

TABLE II Chemical analysis of residual glass at grain boundaries of AD–96 aluminum oxide

Treatment	Composition (mol %)				
	Na_2O	MgO	CaO	Al_2O_3	SiO_2
As-received	5.03 (1.25)*	11.21 (1.63)	2.77 (0.37)	16.11 (0.91)	64.88 (2.33)
Annealed† (unstressed material)	5.05 (0.86)	3.37 (0.35)	3.72 (0.44)	16.09 (0.76)	71.78 (1.80)
Annealed (100 μm thin section)	4.41 (1.85)	2.50 (0.76)	0.66 (0.16)	14.60 (0.96)	77.78 (3.13)
Tensile surface	3.52 (1.44)	2.74 (0.39	0.65 (0.12)	13.42 (0.45)	79.67 (1.49)
Tensile surface	3.66 (1.09)	2.62 (0.04)	0.92 (0.17)	14.13 (0.63)	78.52 (1.65)
Compressive surface	3.61 (0.67)	3.02 (0.65)	0.92 (0.13)	14.70 (0.47)	77.75 (1.42)
Tensile section	2.83 (1.73)	3.03 (0.82	1.97 (0.55)	15.26 (0.90)	76.96 (2.36)
Compressive section	3.24 (1.78)	3.31 (0.72)	3.44 (0.40)	16.48 (1.17)	73.59 (2.46)

*The standard deviation of each measurement is given in parentheses.
†Annealed for 96 h at 1044° C, then subjected to creep for ~ 50 h at an initial applied stress of 60 MPa. The unstressed material was taken from the end of the specimen.

§The chemical composition of members of the plagioclase series is generally given in terms of its pure end-members anorthite (An), $CaAl_2Si_2O_8$ and albite (Ab), $NaAlSi_3O_8$. On this basis, the average composition listed in Table II corresponds to 50% Ab · 50% An, although considerable variations in compositions and a systematic calcium deficiency were observed.

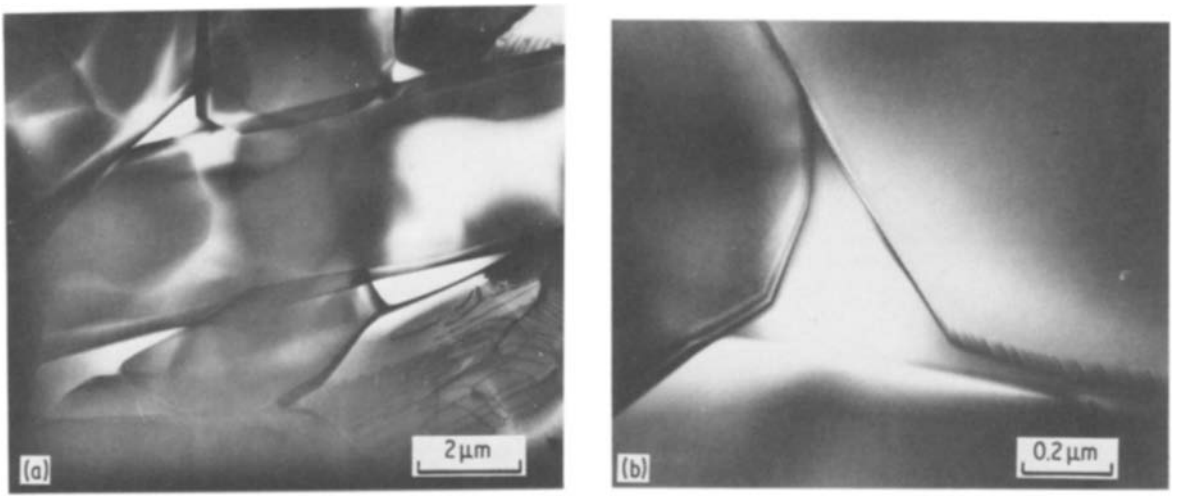

Figure 3 TEM illustrating microstructure of vitreous bonded alumina in as-received condition. (a) Representative view showing non-uniform morphology of aluminium oxide grains and glassy binder phase at triple junctions. (b) Enlarged view of structureless glassy phase at triple junctions and between widely separated grains. Surface faceting of aluminium oxide grains evident in (b) was characteristic feature of vitreous-bonded material.

boundaries and multi-grain junctions (Fig. 4b). Moreover, the additional crystallization of plagioclase within the surface regions results in a retained glass phase composition (Table II) which is more silica-like, and hence is different from the glass phase found within the interior.

To a large extent, analytical electron microscopy results for annealed samples provide a basis for summarizing the differences in microstructures found within samples that were preannealed at 1050° C and then deformed in creep to -0.1% strain at an applied stress of 60 MPa. Particular emphasis is again placed on the intergranular regions, since this is where deformation occurs. With reference to Fig. 1, samples taken from within 100 μm of the tensile and compressive surfaces of deformed samples were virtually indistinguishable from each other and from those from the surfaces of statically annealed samples. In each, the intergranular binder phase was largely crystalline (again estimated as up to 75% of binder phase volume), due to the formation magnesio-aluminosilicates and intermediate plagioclase. From Table II, the compositions of retained glass in the surface intergranular regions were also quite similar. Tensile surface sections were, however, marked by the occasional presence of stoichiometric, orthorhombic cordierite and, in samples where the original surface was retained, by the presence of discrete magnesio-aluminosilicate crystallites along the periphery of two-grain boundaries and multi-grain junctions. By scanning electron microscopy (SEM) these crystallites were determined to lie on the surface, thus indicating a transfer of material from the interior to the tensile surface.

Further examination of deformed samples, using longitudinal cross-sections (Fig. 1), provided clear evidence that the stresses developed during testing have a significant effect on the devitrification process, and hence on the structure and composition of the intergranular bonding phase. Within the tensile regions, extensive devitrification of the glass binder phase resulting in 50 to 70% crystallization, extending to distances of approximately one-fourth the sample thickness, the limit of observations (Fig. 5). In con-

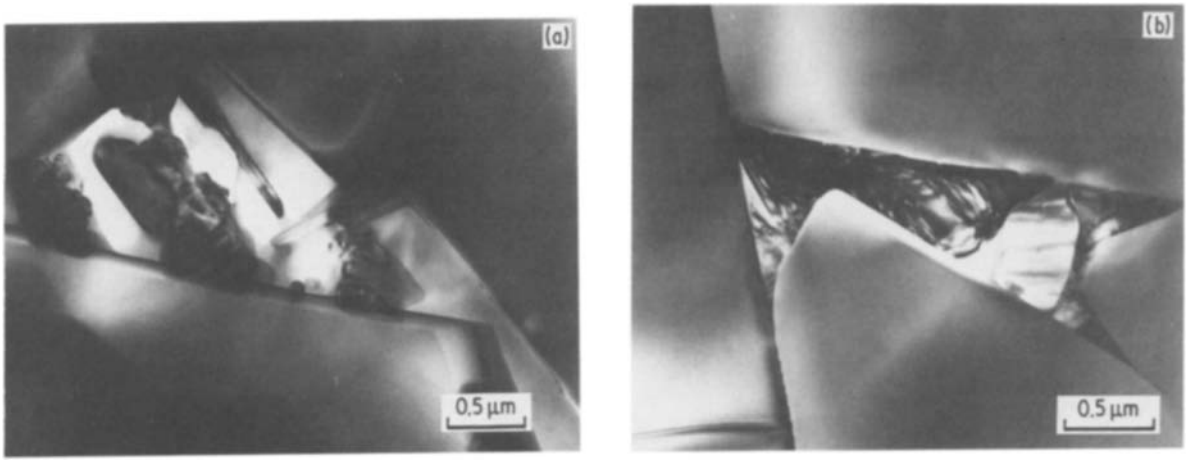

Figure 4 TEM results. (a) Discrete crystallites of magnesio–aluminosilicate phases (see text for description) produced within multi-grain junction after prolonged heat treatment at 1050° C. Nature and extent of crystallization typifies partial devitrification of glassy binder phase that occurs within interior of bulk samples. (b) Fully crystallized integranular structure typically produced within near-surface regions after similar heat treatment. More complete devitrification is related to additional formation of intermediate plagioclase. As described in text, (a) is also typical of compressive subsurface regions and (b) typical of tensile subsurface regions after flexural creep.

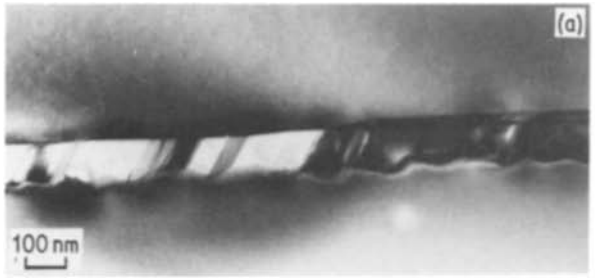

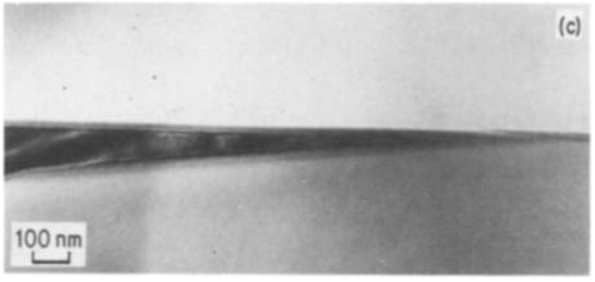

Figure 5 TEM results. Examples of crystallized grain boundary structures, invariably intermediate plagioclase, produced within tensile regions of flexural creep samples.

trast, the degree of devitrification diminished rapidly below the compressive surface, and at a depth corresponding to one-tenth the sample thickness the bonding phase was essentially glassy. Within the compressive regions, the structure and composition of the bonding phase was, in fact, nearly identical to that found within the interior of bulk annealed samples, whereas within the subsurface tensile region it closely resembled that found at the surface. These results suggest a net increase in specific volume of the bonding phase (i.e. the combined volume change of the glass and crystalline phases at the grain boundaries) as a result of the devitrification process. Thus, devitrification would be enhanced in the tensile cross-section of the specimen, and retarded in the compressive cross-section of the specimen.†

Creep samples were also examined for evidence of void or cavity formation within the intergranular phase. In contrast to earlier results for hot-pressed silicon nitride (tested in both tension and compression) [3, 5, 13–15] and for a glass-bonded alumina (tested in compression) [16], definitive evidence for widespread cavitation was not found.‡ Nevertheless, observations on tensile surface regions by SEM (Fig. 6a) clearly showed intergranular cavitation, though it was generally restricted to the neighborhood of well-developed creep cracks. In addition, TEM studies on similar tensile surface sections revealed occasional evidence of grain-boundary delamination in the form of narrow plate-like cavities (Fig. 6b). While it appears clear that grain-boundary delamination eventually leads to the formation of fully developed cracks that are responsible for creep rupture, the necessary conditions and processes involved in crack formation remain the object of continuing study.

3.2. Creep data

Examples of creep data obtained in the present experiments are illustrated in Figs. 7 and 8. There was little indication of Stage 3 creep prior to failure in any of the creep tests. Failure often occurred without any change in the creep rate, suggesting that a second process, such as rapid crack growth, abruptly cuts off the normal creep process in these specimens. Sometimes a slight increase in the creep rate is observed just before

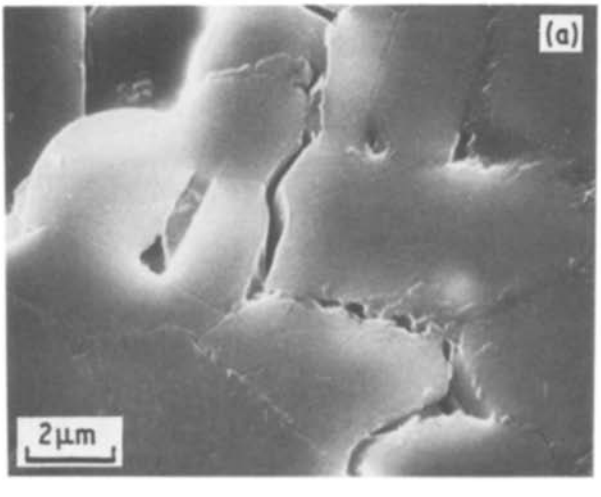

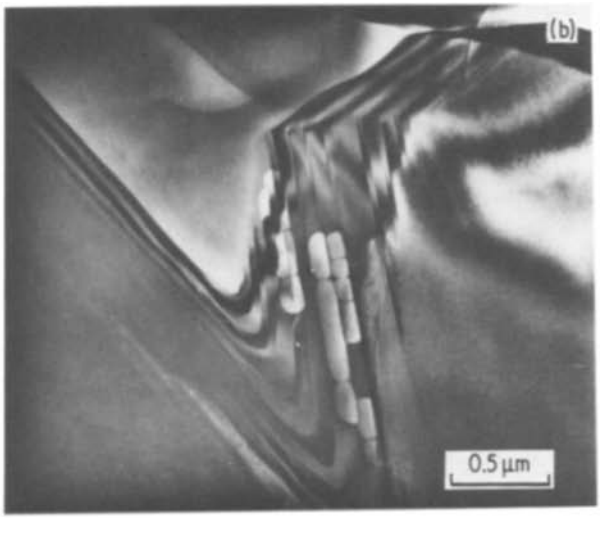

Figure 6 (a) SEM illustrating cavitation at grain boundaries and triple junctions in vicinity of developing creep crack on tensile surface. (b) TEM showing plate-like cavities at inclined grain boundary after creep deformation. Formation and growth of such cavities is considered responsible for intergranular creep crack extension.

†The thermodynamics of devitrification of grain boundaries has been discussed recently in some detail by Raj and Lange [12].
‡While cavity-like holes were often found within multi-grain junctions even in thick regions of TEM samples, they were similarly present in tested and untested samples and are, therefore, attributed to preferential ion-thinning.

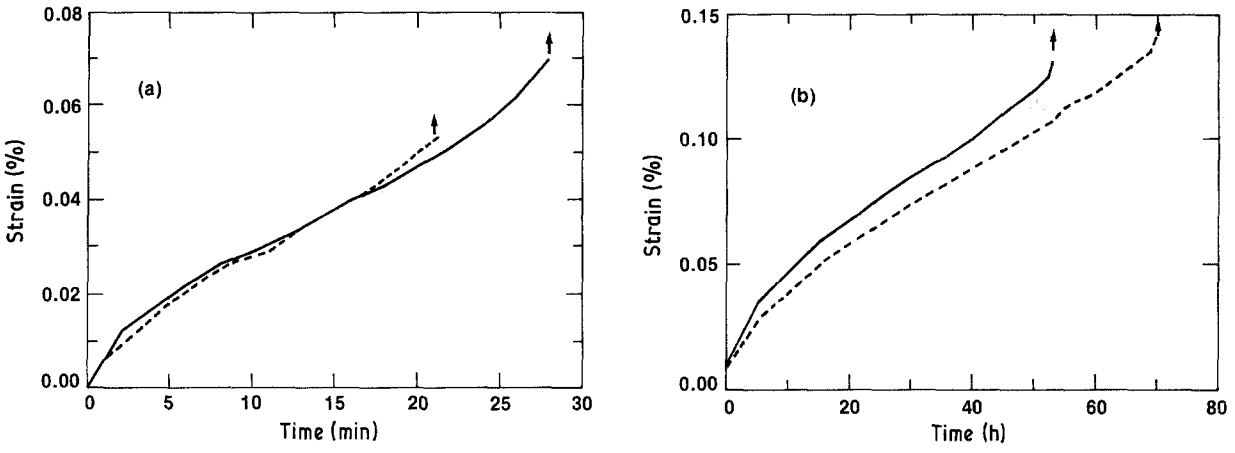

Figure 7 Creep of AD–96 alumina under an applied stress of 60 MPa at 1044° C. (a) No prior annealing. Note that failure occurred within 30 min of initial load application for both specimens. (b) Specimen annealed for 96 h at 1044° C prior to testing. Annealing results in an approximate two hundred-fold increase in specimen lifetime, primarily as a consequence of grain-boundary devitrification.

failure, but the sort of creep-rate enhancement often reported for structural metals does not occur for this ceramic. This slight increase in creep rate is probably due to an increase in specimen compliance resulting from rapid crack growth.

Considerable run-to-run scatter was observed in the failure times for a given test condition, even when specimens were tested simultaneously in the same furnace. Scatter in the failure times by as much as a factor of three was not uncommon. By contrast, the minimum creep rate for a given test condition was relatively constant from run to run. Finally, annealing has an enormous effect on the creep behaviour of this material. The annealing treatment of 96 h at $\sim 1050°$ C decreased the creep rate and increased the lifetime by a factor of almost 100 (Fig. 7). As will be discussed below, this decrease in the creep rate can be directly attributed to devitrification and to the changes in the volume fraction and the viscosity of the glass at grain boundaries.

The creep data illustrated in Figs. 7 and 8 may be summarized by expressing the minimum strain rate, $\dot{\varepsilon}$, as a function of applied stress, σ, and temperature, T:

$$\dot{\varepsilon} = A(\sigma/\sigma_0)^n \exp(-\Delta H/RT) \quad (1)$$

where R is the gas constant and A, n and ΔH are empirically determined constants. The constant A has units of h^{-1} and the normalization constant, σ_0, for the stress has units of MPa. In the present experiment the constants A, n and ΔH were determined by a least-squares fit of Equation 1 to 28 sets of the experimental data. The values of these constants and their standard deviations are $\ln A = 53.6 \pm 5.0$; $n = 4.85 \pm 0.45$; $\Delta H = 926 \pm 58\,\text{kJ mol}^{-1}$. The standard deviation of the fit was approximately ± 0.45.

3.3. Creep-rupture behaviour

The creep-rupture data obtained in the present experiments are summarized in Fig. 9, where the logarithm of the minimum creep rate is plotted as a function of the logarithm of the rupture time. As can be seen from this figure, there is a negative correlation between the minimum strain rate and the time to failure. If the failure time is expressed as a power function of the minimum strain rate, then the data shown in Fig. 9 can be expressed by the following equation:

$$t\dot{\varepsilon}^a = b \quad (2)$$

where the constants and their standard deviations,

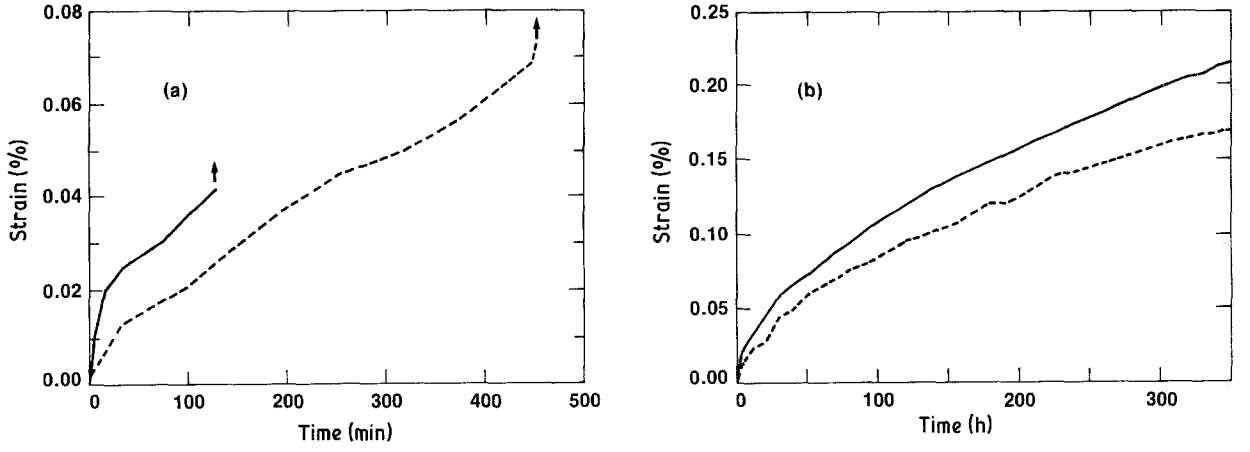

Figure 8 Comparison of short- and long-term creep of AD–96 alumina at 1044° C: initial applied load (a) 80 MPa, (b) 40 MPa. In neither creep measurement could a distinct steady-state region be identified. This is particularly true for the long term runs (b), which suggest continual work-hardening. The upper curve in (b) was in an advanced state of fracture and yet gave no indication of Stage 3 behaviour. In the other creep curves of Figs. 7 and 8, the initial and final stages of creep tend to overlap.

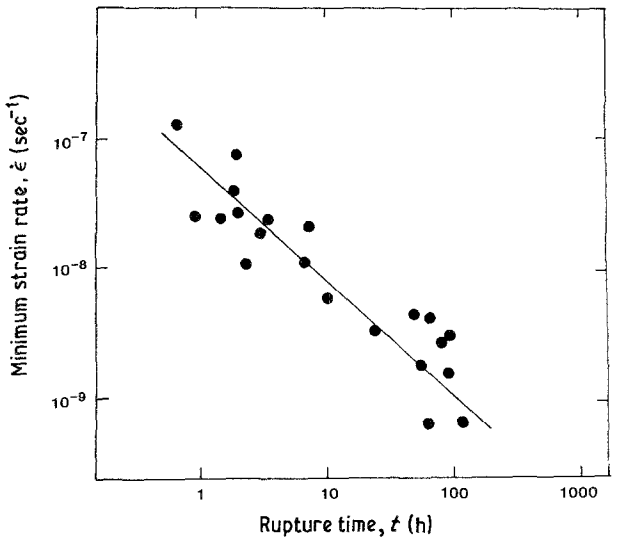

Figure 9 Creep-rupture data fitted to a Monkman–Grant type of plot for AD-96 aluminium oxide.

$a = 1.10 \pm 0.11$ and $\ln b = -8.97 \pm 0.13$, were obtained by a linear regression analysis of $\ln t$ upon $\ln \dot{\epsilon}$ for 21 sets of data. The standard deviation of the fit was approximately 0.72. Equation 2 is the Monkman–Grant [17] equation, first used to describe the creep of metals. The exponent, a, in this equation is not significantly different from 1, the value usually used to describe creep.

The variance of the data about the regression line in Fig. 9 can be reduced significantly if temperature and/or applied stress are introduced as variables. This is illustrated in Fig. 10 where the data from Fig. 9 have been replotted and identified as either constant temperature (Fig. 10a) or constant stress (Fig. 10b) data. In both representations, the data are observed to be layered: the points lie on straight lines of either constant temperature or constant stress. Furthermore, it can be seen that the scatter of the data about the lines, in either representation, appears to be less than that given by the Monkman–Grant relation, indicating the importance of temperature and stress as experimental variables.

The introduction of temperature and applied stress into the analysis can be quantified by assuming that the creep rupture data fit an empirical equation of the following type:

$$t\dot{\epsilon}^a = B\sigma^m \exp(-\Delta H'/RT) \quad (3)$$

By taking the natural logarithm of both sides of the above equation, the equation can be linearized and the constants a, B, m and $\Delta H'$ can be determined by a linear regression analysis of the data. The results of this analysis are given in Table III. A large and significant dependence of $t\dot{\epsilon}$ on applied stress and temperature indicates that some of the variance in Fig. 9 can be attributed to a variation in these two parameters. In fact, the standard deviation of the fit, ± 0.34, is reduced by a factor of approximately one-half by taking temperature and stress into account.

3.4. Strain at failure

Another relationship that can be obtained from the creep-rupture data is that of the maximum strain to failure. In the metals literature, the assumption of a constant maximum strain to failure is often used as a criterion for failure [18]. The unmodified Monkman–Grant relation of Equation 2, for example, is essentially a constant strain to failure criterion. By plotting the strain to failure as a function of other test variables, it should be possible to provide additional data for comparing creep and creep-rupture data with theory.

In Fig. 11, the total strain to failure is plotted as a function of the applied stress.§ Although the scatter of the data is considerable, the figure suggests a negative correlation between these two variables, so that as the stress applied to the specimen is decreased the failure strain is observed to increase. This correlation is supported by data collected on two other specimens loaded at 40 MPa and 1044° C for a period of 350 h. Although they did not fail, the strains on the specimens at the time the tests were discontinued were 0.17 and 0.21%, which were greater than any of the failure strains indicated in Fig. 11. Similar observations were made by Clarke [16], who also noted that failure shown in compressive creep correlated inversely with applied stress.

4. Discussion

4.1. Grain-boundary viscosity

In the temperature range used in the present investigation, all but a few high-silica glasses behave as viscous liquids. Therefore, the glasses at grain boundaries in the present study are also most likely to be liquid, and liquid-enhanced creep undoubtedly dominates the creep results presented in this paper. In all of the theories developed to describe the effect of inter-

TABLE III Summary of creep-rupture data*

$\ln B$	a	m	$\Delta H'$ (kJ mol^{-1})	Standard deviation of fit	Degrees of freedom
−7.95 (0.16)†	1 (assumed)	0 (assumed)	0 (assumed)	0.71	20
−8.97 (0.13)	1.1 (0.1)	0 (assumed)	0 (assumed)	0.72	19
−7.6 (3.6)	1 (assumed)	−4.2 (0.56)	195 (54.0)	0.334	18
−8.0 (7.9)	1.0 (0.1)	−4.2 (0.94)	200 (141.3)	0.344	17

*Data fitted to the logarithmic form of Equation 3: $\ln t = \ln B - a \ln \dot{\epsilon} + m \ln \sigma - \Delta H/RT$.
†Standard deviation given in parentheses.

§The total strain at failure includes that determined from the minimum creep rate ($t\dot{\epsilon}$) and that determined from the transient portion of the creep curve. The total strain ranged from ~1.5 to ~2.5 $t\dot{\epsilon}$.

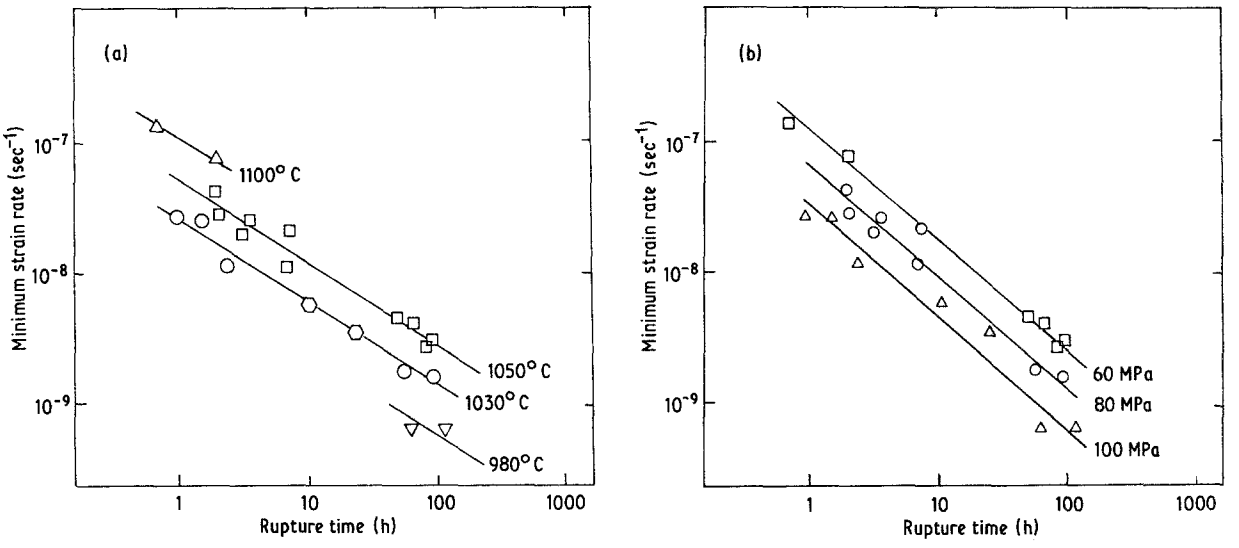

Figure 10 Creep-rupture data for AD–96 plotted as in Fig. 9, but identifying points of either (a) constant temperature, or (b) constant applied stress; (▽) 980° C, (○) 1000° C, (○) 1030° C, (□) 1050° C, (△) 1100° C.

granular liquids on creep deformation, the viscosity of the liquid is an important variable which should be evaluated to fully understand the creep process. Therefore, in this section the viscosity of the intergranular glass is calculated from its composition. In the next section, these calculated viscosities are used to evaluate mechanisms of creep.

The viscosities of the vitreous grain-boundary phases were estimated from the compositions given in Table III, by using empirical equations developed by Urbain *et al.* [19] for this purpose. These equations were developed from experimental data on a series of calcia–alumina–silica glass melts, and were tested on a number of slags and glasses for which the equations gave values of viscosity that agreed with experimental measurements to within a factor of 5 [20]. The equations were, however, developed for the low viscosity range $< 10^4$ Pa sec, so that agreement between these equations and experimental data is not expected over the entire range of viscosities.

Before using the equations of Urbain *et al.* [19] on the present set of data, the equations were applied to commercial glasses with known compositions and viscosities. The glasses selected for comparison were made by the Corning Glass Works (Houghton Park, Corning, New York) and have the composition indicated in Table I [21]. The calculated and experimental values of the viscosity for C0080 glass, (Fig. 12) agree to within an order of magnitude for the viscosity range 10^{11} Pa sec (530° C) to 10^2 Pa sec (1000° C), which was almost the entire practical range of viscosities for annealing and forming this glass. For C1720 (Fig. 12) an order-of-magnitude agreement between calculated and measured viscosity is obtained for viscosities lying between 10^7 Pa sec (900° C) and 1 Pa sec (1200° C).

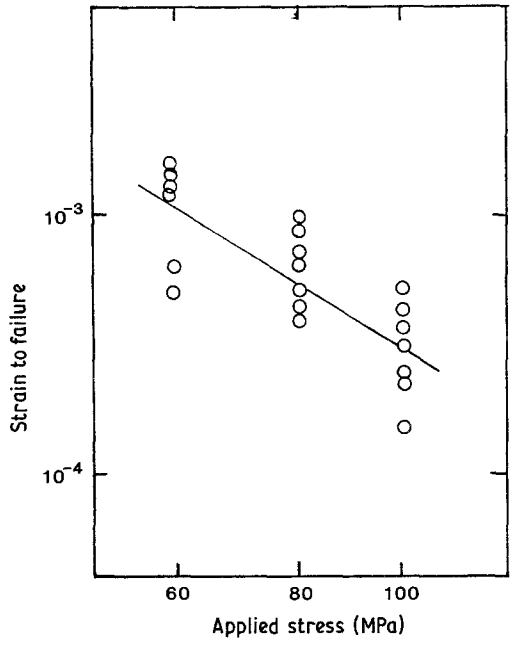

Figure 11 Strain to failure as a function of initial applied stress.

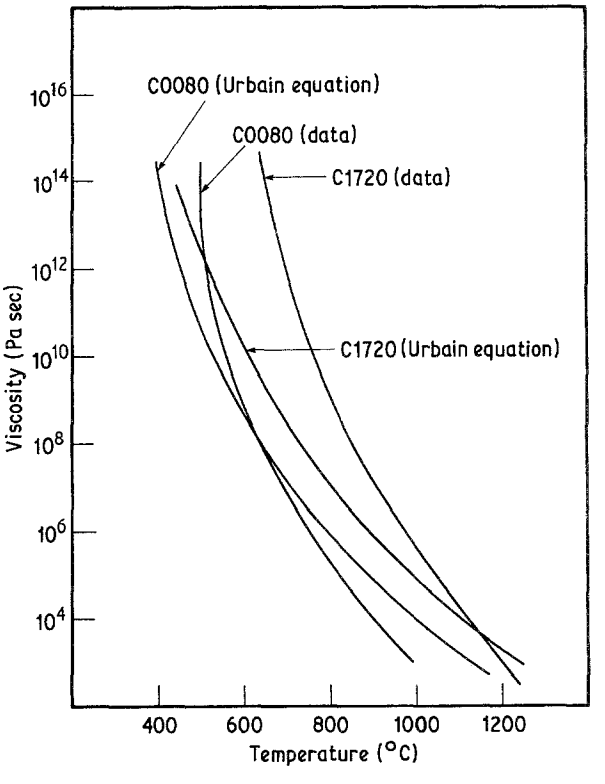

Figure 12 Viscosity of two commercial glasses compared with viscosities calculated from the equations of Urbain *et al.* [19].

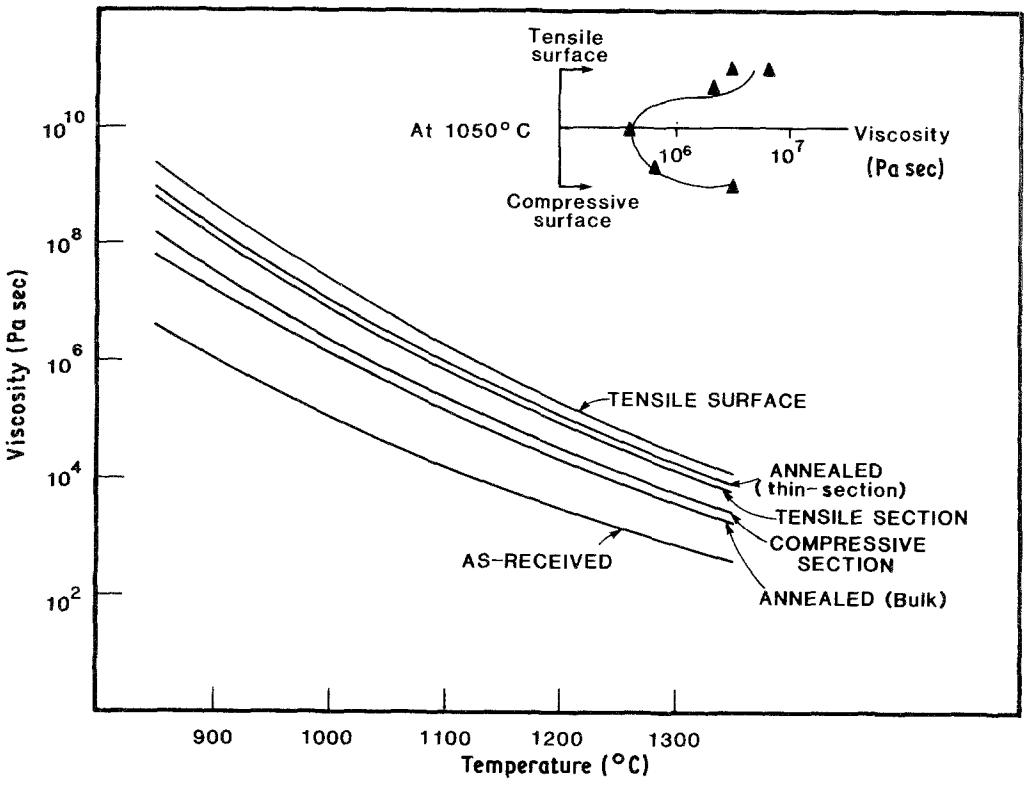

Figure 13 Calculated viscosities of glass composition given in Table III. The insert shows how the glass viscosity changes from the tensile to the compressive cross-section of the bend bars at a temperature of 1044° C.

This agreement between calculated and measured viscosities is considered reasonable for the present study.

The viscosities of the glass compositions given in Table III are shown in Fig. 13. The figure demonstrates the rather sizeable effect of annealing and deformation on the viscosities of these glasses. At any given temperature, changes by a factor of ten in viscosity are observed as a consequence of annealing and creep deformation. This increase in glass viscosity should reduce the creep rate of the annealed specimens by a commensurate amount, because the creep rate is inversely proportional to the viscosity in most theories of creep. Similarly, the additional factor of ~ 10 increase in the glass viscosity in both the tensile and compressive surfaces of the annealed specimens suggests that the surface of the specimens are more resistant to creep than the body of the specimens. This finding raises the possibility of surface embrittlement as a consequence of devitrification during annealing.

The difference in composition of the glass in the tensile and compressive cross-sections suggests a difference in viscosity of the glasses in these cross-sections. Using the formulation of Urbain *et al.* [19], the viscosity of the glass in the tensile cross-section is calculated to be approximatly a factor of three greater than that in the compressive cross-section. The presence of crystalline material at the grain boundaries of the tensile cross-section magnifies the viscosity difference even further, so that the effective viscosity of grain boundaries that have been devitrified will be greater than that indicated by the viscosity of the glass alone. Thus, the effective viscosity of the material at the grain boundaries in the tensile cross-section should be more than a factor of three greater than the effective viscosity of the material at the grain boundaries of the compressive cross-section.

These effects of composition on viscosity have interesting implications with regard to the effects of the state of stress on the creep rate. If the effective grain-boundary viscosity were the sole determinant of creep rate, then one would expect tensile specimens to be more creep-resistant than compressive test specimens, for an equivalent temperature and applied stress. In fact, experimental studies on this subject reach the opposite conclusion; creep occurs more easily in tension than in compression [22]. Therefore, while grain-boundary viscosity is important, it is not the only physical or structural parameter determining the creep rate. The overall rheology of the test specimen *vis-à-vis* the state of stress must also be considered. Creep no doubt depends on details of the microstructure such as level of agglomeration, level of homogeneity and amount of direct contact between grains of the microstructure. These effects of microstructure have not yet been considered for ceramic materials. In fact, most theories of creep assume a homogeneous microstructure, an assumption that is clearly not consistent with the structure of most materials investigated. Thus, while intergranular viscosity is probably of paramount importance in determining the creep rate of a component subjected to a particular state of stress, other factors must be considered when the state of stress is a variable.

The effect of devitrification on the creep rate can be quantified by comparing the creep rate of the annealed specimens with that of the as-received specimens. At 1044° C and an initial applied load of 60 MPa, a hundred-fold decrease in the creep rate is observed upon annealing the specimens. Based on most theories of creep, this result suggests a factor of 100 decrease in the effective grain-boundary viscosity. Since the viscosity of the glass at the grain boundaries decreases by

only a factor of ten due to annealing, a change in glass composition alone cannot explain the decrease in creep rate. Crystallization of the grain boundaries effectively increases the average viscosity of the grain-boundary phase by another factor of ten, and in this way decreases the creep rate of the specimens.

4.2. Models of creep

The simplest model of liquid-enhanced creep is that of lubricated flow wherein the grain-boundary glass behaves as a lubricant, reducing the friction between grains. For an applied deviatoric stress $\bar{\sigma}$, the creep rate $\dot{\varepsilon}$ is given as a function of grain size d, grain boundary thickness w and viscosity η [23]:

$$\dot{\varepsilon} = \alpha\left(\frac{w}{w+d}\right)\left(\frac{\bar{\sigma}}{\eta}\right) \quad (4)$$

where α is a constant having a value of approximately $\frac{1}{3}$. Substituting $\bar{\sigma} = 40\,\text{MPa}$, $d = 8\,\mu\text{m}$, $\eta = 10^6\,\text{Pa sec}$ (the value for the annealed specimen at 1040° C) into Equation 1, we obtain a calculated value of the grain boundary thickness, w, of $1.8 \times 10^{-15}\,\text{m}$ for a creep rate of $3 \times 10^{-9}\,\text{sec}^{-1}$ (60 MPa applied stress, 1040° C). This estimated value of w is of course subatomic, indicating that frictional forces at grain boundaries provide almost no impediment to the creep process. Therefore, lubricated flow cannot possibly be an acceptable mechanism for the creep results in the present study. As noted by others [23, 24], lubricated flow is probably never an explanation for liquid-enhanced creep because the mechanism does not take into account the complexity of the microstructure for most materials. Grains that form the microstructure do not lie in ordered planes, as assumed in the model of lubricated flow. When subjected to stress, grains tend to lock up as the solid is deformed, greatly increasing the forces required to maintain a given rate of creep. In this way, the material work-hardens. For flow to continue, i.e. for the grains to slide over one another, an increase in the volume (a dilatation) must occur [25, 26]. Therefore, if liquid lubrication were the only possible process, creep would become more and more difficult as the strain increased and the creep would eventually stop. In fact, creep continues because there are mechanisms of accommodation that relieve the stresses caused by the volume expansion. In the order to be discussed below these mechanisms include (a) fluid flow or percolation, (b) pressure solution or solution precipitation, and (c) grain-boundary cavitation.

Percolation, or fluid flow, was first mentioned as a mechanism of accommodation by Reynolds [25], and later by Frank [26]. The effect of fluid flow on creep was quantified by Drucker [27] and by Lange [24], who calculated the rate of creep resulting from the localized flow of liquid from the compressive to the tensile surfaces of individual grains. The equation developed by Drucker for the strain rate is

$$\dot{\varepsilon} = \left(\frac{\sigma}{\eta 3^{1/2}}\right)\left(\frac{w}{d}\right)^3 \quad (5)$$

where σ is the applied tensile or compressive stress. The model assumes that the grains lie in a two-dimensional hexagonal array and that flow is homogeneous throughout the material. Substituting experimental values of η ($10^6\,\text{Pa sec}$), σ (60 MPa) and d ($8\,\mu\text{m}$) into this equation yields the following relation between $\dot{\varepsilon}$ and w: $\dot{\varepsilon}/w^3 = 6.7 \times 10^{16}\,\text{sec}^{-1}\,\text{m}^{-3}$, from which a grain-boundary thickness of 3.5 nm is calculated for a creep rate of $3 \times 10^{-9}\,\text{sec}^{-1}$ at 1044° C. This value of the grain-boundary thickness lies at the lower end of the range normally observed for glass-bonded aluminum oxide, which suggests that a significant resistance to fluid flow only occurs along the narrowest boundaries of the composite. During deformation, glass flows easily from pores or external surfaces along triple junctions and therefore wide grain boundaries offer little resistance to fluid flow. By contrast fluid flow along narrow grain boundaries is difficult, so that the local stresses will be greatest along these boundaries. Because of these preferred paths for fluid flow, deformation of polyphase materials is most likely non-homogeneous. Devitrification increases the difficulty of fluid flow by increasing the effective grain-boundary viscosity by a factor of approximately ten over that calculated for the glass in the annealed specimens. This increase in viscosity should increase the estimate of the grain-boundary thickness by a factor of approximately two.

Turning now to solution precipitation as a means of liquid-enhanced creep, two types of mechanism have been suggested. In one, the grains of the solid are in firm contact and the driving forces for solution and precipitation result from the high stress that occurs at contact points [23, 28, 29]. The creep rate can then be limited either by the kinetics of solution and precipitation, or by the rate of transport from regions of high to regions of low stress, the transport processes being driven by the gradient of the chemical potential and its dependence on pressure. These mechanisms were discounted in the present experiments because no evidence of intergranular contact was found in microstructural analyses of deformed specimens. If contact sites were present they would appear as well-defined regions of strain contrast, as has been reported by Lange *et al.* [30] in TEM studies of hot-pressed silicon nitride. Similar patterns of strain contrast due to intergranular contact have been observed in hot-pressed silicon nitride in our own laboratory [31]. In the glass-bonded aluminum oxide, however, no such strain contrast was observed at grain boundaries in the present study. Therefore, either the contact sites were not there, or they were so widely spaced that their observation would have been rare. In this section we assume that the grains were not in contact, and that each grain of solid was completely surrounded by glass.

When glass forms a continuous phase around the grains, then stress gradients within the glass result from the high viscosity of the glass, which resists the imposed forces and prevents the grains from touching. Solution reprecipitation for this situation has been analysed by a number of investigators [32–35], and creep equations similar to the following one by Rutter [34] have been reported for transport limited processes:

$$\dot{\varepsilon} = \frac{32\sigma V C_0 D w}{N_0 k T \varrho d^3} \quad (6)$$

where V is the molar volume of the solid (Al_2O_3), C_0 is the concentration (mass vol^{-1}) of the diffusing species in the solution, D is the diffusivity, N_0 is Avogadro's constant, k is Boltzmann's constant and ϱ is the density of the solid.

In our treatment of creep by solution precipitation, the diffusivity must be estimated in order to evaluate the creep rate. Usually, the Stokes–Einstein relation ($D = kT/6\eta\pi r$) is used in solution precipitation theories to estimate the diffusivity in terms of the liquid viscosity, η, and the radius, r, of the diffusing species. Whereas the Stokes–Einstein relation works well for liquid metals and molten salts, problems are encountered in its application to liquids, such as glasses and polymeric melts, that have a network structure [36]. In these structures, most atoms diffuse through the network. By contrast, viscous flow is determined primarily by the structure of the network, i.e. by the breaking of network bonds, so that the two processes may not be closely related, and consequently the errors in estimating the diffusivity can be large [36, 37]. Thus, before using the Stokes–Einstein relation, its potential for error should be recognized and if possible the equation should be assessed on known sets of data.

In the present investigation the transport of aluminum ion, Al^{3+}, probably controls aluminum oxide diffusion, because its rate of diffusion is much less than that of oxygen, O^{2-}, in silicate melts [38, 39]. To test the applicability of the Stokes–Einstein relation to Al^{3+}, experimental parameters for viscosity and diffusivity assembled by Cooper and Kingery [39] were used. At 1400° C the diffusivity of Al^{3+} is $\sim 2.6 \times 10^{-7}\,cm^2\,sec^{-1}$, while the viscosity is 23.3 poise (2.33 Pa sec), from which an ionic radius of ~ 0.02 nm is calculated. This value is about a factor of 2.5 smaller than that (0.05 nm) estimated by Pauling [40] from wave-mechanical considerations. The diffusivity and the viscosity also appear to have similar temperature dependencies ($\Delta H = \sim 272\,kJ\,mol^{-1}$ for diffusion and $\sim 229\,kJ\,mol^{-1}$ for viscous flow). Based on this comparison, the Stokes–Einstein relation is expected to give an order-of-magnitude estimate for the diffusivity of Al^{3+} in the temperature range used for the present study.

Substituting the Stokes–Einstein equation into Equation 6, the following relation is obtained for the creep rate:

$$\dot{\varepsilon} = \frac{32\sigma V C_0 w}{6 N_0 \eta r \varrho d^3} \quad (7)$$

Using appropriate experimental values ($V = 25.5\,cm^3\,mol^{-1}$, $C_0 = 0.625\,g\,cm^{-3}$, $r = 0.02$ nm, $\varrho = 4\,g\,cm^{-3}$) in Equation 7, the relation between $\dot{\varepsilon}$ and w is given by $\dot{\varepsilon}/w = 8.7 \times 10^{-2}\,sec^{-1}$, from which a grain-boundary thickness of 34 nm is calculated for an initial applied stress of 60 MPa at a temperature of 1044° C. This grain-boundary thickness lies within the range of values observed in the present experiment. In view of the assumptions made in obtaining this number, the fact that this estimate of grain-boundary thickness is an order of magnitude greater than that for percolation with the same experimental parameters cannot be considered significant. Within the accuracy of the models and the material property estimates, therefore, the solution precipitation and the percolation models of creep must be considered competitive.

Nucleation and growth of cavities within grain boundaries provides a third mechanism by which work-hardening resulting from the dilatant behaviour of the polycrystalline solid can be relieved. Cavitation is commonly observed as a means of accommodation in metals, and has been reported in a number of studies for ceramics tested in tension, bending and compression [3, 5, 13–16, 20]. Since homogeneous cavitation was not observed in the present study it must be concluded that cavity formation and growth did not play a major role during creep deformation. This conclusion is very different from that reached by Clarke [16], who found that high-temperature deformation of glass-bonded alumina was dominated by cavitation within the glass phase. The reasons for the difference between our results and Clarke's are not fully understood at the present time, but may reside in differences in the composition and viscosity of the glasses used in the two studies. Although the two studies were conducted over roughly the same temperature range, the viscosity of the glass bonding phase in Clarke's study was approximately two orders of magnitude less than in our own study. In fact, the viscosity of the glass used by Clarke [16] was similar to that of the glass in the unannealed specimens in our study. Further studies are indicated to clarify the role of cavitation in the creep process, and the conditions under which cavitation occurs in two-phase ceramics.

Although extensive cavity nucleation, of the type reported in the creep-rupture literature, was not observed in the present study, isolated and fairly widely spaced grain-boundary delaminations were observed. The delaminations occurred at the tensile surface where the stresses were highest, and where the surfaces were embrittled by extensive devitrification of glass at the grain boundaries. These delaminations form preferentially at two grain boundaries where, according to percolation theories of creep, the stresses are highest. These delaminations may be precursors of cracks that nucleate in the tensile surface of the specimen and grow to a critical size during the course of the creep experiment.

4.3. Creep and creep-rupture phenomenology

Although the initial purpose of this study was to estimate the creep behaviour of a two-phase ceramic from an analysis of the microstructure of the ceramic, the extensive collection of creep and creep-rupture data presented in this paper warrants some brief comment on the data and its comparison with other data of the same type. In this section, discussion is limited to vitreous-bonded oxides including refractories, porcelains and glass–ceramics, which are closest in structure to the material used in the present study.

4.3.1. Stress exponent

In the present paper the classical power-law creep expression given by Equation 1 was fitted to the creep data. Both the power-law exponent, $n = 4.85$, and the apparent activation enthalpy, $\Delta H = 926\,\text{kJ mol}^{-1}$, lie at the high end of values reported for creep processes. Literature values of n range from ~ 1 to 6 depending on the material tested and the level of stress [6, 7, 22, 41, 42]. The value of n tends to increase as the stress is increased, but does not appear to depend on the sign of the applied stress, i.e. whether the applied stress is tensile or compressive [20]. In view of these comments, the value of n obtained in the present experiments is not unusual, even though it lies at the high end of the range of values.

Since most theories of creep are linear in applied stress ($n = 1$) they cannot be used in unaltered form to explain non-linear aspects of creep or creep rupture. Most often, investigators have suggested cavitation or microcrack formation as the primary explanation for a high creep exponent [3, 22]. As cavities are formed the applied stress is transferred from the cavitated to the uncavitated portion of the specimen, and the creep rate increases as a result of both cavity nucleation and cavity growth. Since the rate of nucleation and growth of cavities is basically a non-linear function of applied stress [14], the creep process is also a non-linear function of stress. Thus, Moreel and Ashbee [22], Lange *et al.* [3], Clarke [16] and others have used cavitation as a means of explaining the non-linear dependence of creep on stress.

In the present experiments, no evidence of cavitation at grain boundaries was obtained, and therefore it is difficult to explain the non-linear creep behaviour by cavitation. Instead other time-dependent processes such as devitrification and premature termination of the creep process by fracture are probably responsible for the observations. The importance of crystallization or devitrification was first noted by Norton [6] in a study of the tensile creep of porcelain. Devitrification increases the effective viscosity of the grain-boundary phase and hence increases the resistance of a two-phase material to creep deformation. Norton [6] noted that when crystallization has sufficient time to occur, as when the applied loads are low, then the changes in the microstructure increase the amount of work-hardening and reduce the apparent steady state creep rate. The converse is true at high loads, when creep is rapid and devitrification does not have sufficient time to occur. In this case, the apparent steady state creep rate is higher than would be determined from a linear dependence of creep rate on applied load.

In addition to the structural effects discussed above, premature termination of the creep process by specimen fracture can also play a role in establishing a high value of the creep exponent n. When crack nucleation and crack growth are strongly dependent on the applied stress, then the time to failure may depend on the applied stress in a way that is independent of the creep process. At high levels of applied load, failure is likely to occur in an early stage (i.e. Stage 1) of the creep process, so that the creep rate will be greater than that obtained if creep were not interrupted by fracture. By contrast, failure at low levels of applied stress is likely to occur much later in the creep process (i.e. Stage 2) so that the two measured creep rates will not correspond to the same portion of the creep curve. The net effect of representing such a set of data by Equation 1 is to obtain a non-linear dependence of creep rate on applied stress.

In the present experiments both devitrification and premature specimen failure played a role in establishing the high value of n. Creep occurs initially in a "crack-free" condition; the specimen deforms, work-hardens, and then at some point in time grain-boundary delamination results in crack formation and eventually in specimen failure. The minimum creep rate achieved during each run depends both on the devitrification process, and on the crack nucleation and growth process, both of which lead to a non-linear dependence of the creep rate on applied stress.

4.3.2. Apparent activation enthalpy

Based on the discussions in Sections 4.1 and 4.2, the temperature dependence of the creep rate might be expected to be determined primarily by the glass viscosity, and the dependence of the glass viscosity on composition. For the glass compositions given in Table II, the apparent activation enthalpy for viscous flow is estimated to be $\sim 330\,\text{kJ mol}^{-1}$. This estimate can be increased somewhat by taking into account changes in glass composition that result from changes in temperature. The magnitude of this effect is inferred from the net change in composition due to annealing. From Fig. 13, annealing results in approximately two orders of magnitude increase in viscosity, which should increase the estimated value of the apparent activation enthalpy for viscous flow from ~ 330 to $\sim 550\,\text{kJ mol}^{-1}$, a value that is clearly not enough to explain the high apparent activation enthalpy, $926\,\text{kJ mol}^{-1}$, for creep in the present experiment.

This lack of agreement between the estimated and measured activation enthalpies clearly indicates that factors other than glass viscosity play a role in establishing the temperature dependence of the creep process. Grain-boundary devitrification may be one such factor, since it is known to occur during creep and should have a dramatic influence on the effective viscosity of the grain boundaries. If grain-boundary devitrification is important, then the enthalpy of solution of grain-boundary phases will contribute to the apparent activation ehthalpy of the creep process. The importance of the heat of solution in the creep process has been suggested by Raj and Morgan [43] for a number of high-temperature processes in hot-pressed silicon nitride, and has been applied by Wang and Raj [44] to explain the high activation energies ($\sim 700\,\text{kJ mol}^{-1}$) for the creep of glass–ceramics. The heat of solution is also important when solution precipitation occurs during creep. Further studies will be required to fully elucidate the importance of grain-boundary devitrification in the creep of multiphase ceramics.

4.3.3. Creep rupture

The creep-rupture data shown in Figs. 10 and 11 were found to fit the modified Monkman–Grant relation given by Equation 3. This equation was selected to represent the creep-rupture data because theoretical work by Evans and Blumenthal [45, 46] have been represented in this format. Furthermore, the creep-rupture experiments presented by Johnson *et al.* [47] on direct-bonded aluminum oxide have been shown to fit this type of equation. In this regard, it may be significant that the stress exponent of $t\dot{\varepsilon}$ obtained by Johnson *et al* [47], -6 ± 2, is close to the value obtained in our own experiments, -4.2 ± 0.9, despite the great difference in the microstructures of the two materials.

Most theories that have been developed to describe the creep rupture of polycrystalline systems assume a rather simple microstructure. For two-phase ceramics, the microstructure is usually viewed as a collection of equiaxed grains separated by a viscous fluid [14, 45, 48]. For this type of material, models of crack nucleation, crack coalescence and crack growth have been developed. Generally, these predict a small dependence of $t\dot{\varepsilon}$ on applied stress. To be more specific, $t\dot{\varepsilon}$ for nucleation-controlled creep rupture is predicted to be stress-independent. In view of this prediction, crack nucleation cannot be considered rate-limiting in the present study. For crack-growth controlled fracture, $t\dot{\varepsilon}$ is proportional to σ^{n-p}, where n is the stress exponent for creep and p is the stress exponent for crack growth.* From theoretical considerations, Tsai and Raj [48] suggest $p \leqq 4$ for crack propagation in two-phase materials. Combining $p = 4$ with the value $n = 4.85$ measured in the present paper yields a value for the stress exponent of $t\dot{\varepsilon}$, 0.85, which is not consistent with the experimental results of the present paper. Thus, crack growth alone cannot be used to rationalize the present set of creep-rupture data. The remaining theory of creep rupture, the coalescence theory, is not sufficiently developed to be compared with the present set of data [51].

From the above discussion we must conclude that the theories of two-phase creep fracture that have been developed to date are not able to explain the stress dependence of $t\dot{\varepsilon}$ for the current set of data. In view of the complexity of the material used in the present investigation, this finding is not, perhaps, surprising. Alteration of the material by stress-dependent devitrification undoubtedly plays a role in both the nucleation and crack-growth processes. Additional theoretical work is clearly needed to model the effect of devitrification on crack growth and crack nucleation. In addition, microscopic studies will be needed to elucidate the importance of nucleation and of subcritical crack growth to the failure process.

5. Summary

This paper presents the results of an investigation of the creep and creep rupture of a commercial grade of glass-bonded aluminum oxide. Analytical electron microscopy was used to evaluate the chemical composition of glass at the grain boundaries, and the variation of the composition of the glass with exposure to elevated temperature and creep deformation. The type and degree of devitrification that occurred during creep clearly appeared to be stress-dependent. The glass at grain boundaries in the tensile cross-section of the test specimens was approximately three times as viscous as the glass in the compressive section of the test specimen. This finding is consistent with the pattern of devitrification observed in these specimens. Devitrification was greatest at the tensile surface, which suggests an embrittlement of the surface compared with the rest of the specimen cross-section.

The viscosity of the glass at the grain boundaries was estimated from its chemical composition and was used to compare the measured creep rates in the present study with models that have been developed to describe creep in two-phase ceramics. The creep mechanisms that most closely represent our results are the viscous flow (percolation) mechanism and the solute precipitation mechanism, both of which were suggested by a number of authors. Cavitation was discounted because of the lack of evidence for homogeneous cavitation in the tensile portions of the bend specimens. During later stages of creep, however, grain-boundary delaminations were observed at the tensile surfaces and are probably the origins of cracks that are eventually responsible for the failure of these specimens. Additional studies were recommended to clarify the relative importance of crack nucleation and crack growth to the creep-rupture process.

Acknowledgements

This work was jointly supported by the Department of Energy (Fossil Energy Program) and by the Department of Defense (Air Force Office of Scientific Research).

References

1. E. M. LENOE, R. N. KATZ and J. J. BURKE, (eds.), "Ceramics for High-Performance Applications III, Reliability" (Plenum Press, New York, 1983).
2. Proceedings of the Educational Symposium on Refractories in Slagging Environments, published in *Ceram. Eng. Sci. Proc.* **2**(11–12) (1981).
3. F. F. LANGE, B. I. DAVIS and D. R. CLARKE, *J. Mater. Sci.* **15** (1980) 601.
4. *Idem, ibid.* **15** (1980) 616.
5. R. KOSSOWSKY, D. G. MILLER and E. S. DIAZ, *ibid.* **10** (1975) 983.
6. F. H. NORTON, *J. Amer. Ceram. Soc.* **19**(5) (1936) 129.
7. C. D. HULSE and J. A. PASK, *ibid.* **49**(6) (1966) 312.
8. K. JAMES and K. H. G. ASHBEE, *Prog. Mater. Sci.* **21** (1975) 1.
9. G. W. HOLLENBERG, G. R. TERWILLIGER and R. S. GORDON, *J. Amer. Ceram. Soc.* **54** (1971) 196.
10. G. QUINN and R. KATZ, *Amer. Ceram. Soc. Bull.* **57** (1978) 1057.
11. G. CLIFF and G. H. LORIMER, *J. Micros.* **103** (1975) 203.
12. R. RAJ and F. F. LANGE, *Acta Metall.* **29** (1981) 1993.
13. M. H. LEWIS, B. S. B. KARUNARATNE, J. MERIDITH and C. PICKERING, in "Creep and Frac-

*This relation is obtained by assuming that creep and crack growth are independent processes, so that the time to failure t is given by $t = Bs^{p-2}\sigma^{-p}$ [49] and the creep rate is given by Equation 1. By combining Equation 1 with the equation for t, the relation between $t\dot{\varepsilon}$ and σ is obtained. The idea of simultaneous creep and crack growth was first presented by Lange [50].

ture of Engineering Materials and Structures", edited by B. Whilshire and D. R. J. Owens (Pineridge Press, Swansea, 1981) p. 365.
14. J. E. MARION, A. G. EVANS, M. D. DRORY and D. R. CLARKE, *Acta Metall.* **31** (1983) 1445.
15. N. J. TIGHE, S. M. WIEDERHORN, T.-J. CHUANG and C. L. McDANIEL, in "Deformation of Ceramic Materials II", Materials Science Research, Vol. 18, edited by R. E. Tressler and R. C. Bradt (Plenum Press, New York, 1984) p. 587.
16. D. R. CLARKE, *J. Mater. Sci.* **20** (1985) 1321.
17. F. C. MONKMAN and N. J. GRANT, *Proc. ASTM* **56** (1956) 593.
18. R. W. HERTZBERG, "Deformation and Fracture Mechanics of Engineering Materials", (Wiley, New York, 1976) p. 164.
19. G. URBAIN, F. CAMBIER; M. DELETTER and M. R. ANSEAU, *Trans. J. Br. Ceram. Soc.* **80** (1981) 139.
20. R. C. STREETER, E. K. DIEHL and H. H. SCHOBERT, *Amer. Chem. Soc. Fuel Div. Repr.* **28**(4) (1983) 174.
21. J. R. HUTCHINS, III and R. V. HARRINGTON, in "Encyclopedia of Chemical Technology", 2nd edn, edited by Kirk and Othmer, Vol. 10, (Wiley, New York, 1966) p. 533.
22. R. MORRELL and K. H. G. ASHBEE, *J. Mater. Sci.* **8** (1973) 1253.
23. G. M. PHARR and M. F. ASHBY, *Acta Metall.* **31** (1983) 129.
24. F. F. LANGE, in "Deformation of Ceramic Materials", edited by R. C. Bradt and R. E. Tressler (Plenum Press, New York, 1975) p. 361.
25. O. REYNOLDS, *Phil. Mag.* **20** (1885) 469.
26. F. C. FRANK, *Rev. Geophys.* **3** (1965) 485.
27. D. C. DRUCKER, in "High Strength Materials", edited by V. F. Zackay (Wiley, New York, 1965) p. 795.
28. R. RAJ, *J. Geophys. Res.* **87** (1982) 4731.
29. R. RAJ and C. K. CHYUNG, *Acta Metall.* **29** (1981) 158.
30. F. F. LANGE, D. R. CLARKE and B. I. DAVIS, *J. Mater. Sci.* **15** (1980) 611.
31. N. J. TIGHE, unpublished data.
32. D. W. DURNEY, *Nature* **235** (1972) 315.
33. *Idem, Phil. Trans. R. Soc.* **A283** (1976) 229.
34. E. H. RUTTER, *ibid.* **A283** (1976) 203.
35. R. L. STOCKER and M. F. ASHBY, *Rev. Geophys. Space Phys.* **11** (1973) 391.
36. E. T. TURKDOGAN, "Physicochemical Properties of Molten Slags and Glasses" (The Metals Society, London, 1983).
37. R. H. DOREMUS, in "Modern Aspects of the Vitreous State", Vol. 2, edited by J. D. Mackenzie, (Butterworths, London, 1962) p. 1.
38. R. TERAI and R. HAYANIC, *J. Non-Cryst. Solids* **18** (1975) 217.
39. A. R. COOPER, Jr. and W. D. KINGERY, *J. Amer. Ceram. Soc.* **47**(1) (1964) 37.
40. L. PAULING, "Nature of the Chemical Bond", 3rd edn. (Cornell University Press, Ithaca, 1960) p. 514.
41. F. H. CLEWS, H. M. RICHARDSON and A. T. GREEN, *Trans. Br. Ceram. Soc.* **15** (1945) 161.
42. S. E. BOLD and G. W. GROVES, *J. Mater. Sci.* **13** (1978) 611.
43. R. RAJ and P. E. D. MORGAN, *J. Amer. Ceram. Soc.* **64** (1981) C-143.
44. J.-G. WANG and R. RAJ, *ibid.* **67** (1984) 399.
45. A. G. EVANS and W. BLUMENTHAL, in "Fracture Mechanics of Ceramics", Vol. 6, edited by R. C. Bradt, A. G. Evans, D. P. H. Hasselman and F. F. Lange (Plenum Press, New York, 1983) p. 423.
46. *Idem*, in "Deformation of Ceramic Materials II', Materials Science Research, Vol. 18, edited by R. E. Tressler and R. C. Bradt (Plenum Press, New York, 1984) p. 487.
47. S. M. JOHNSON, B. J. DALGLEISH and A. G. EVANS, *J. Amer. Ceram. Soc.* **67** (1984) 759.
48. R. L. TSAI and R. RAJ, *Acta Metall.* **30** (1982) 1043.
49. J. E. RITTER, Jr., in "Fracture Mechanics of Ceramics", Vol. 4, edited by R. C. Bradt, D. P. H. Hasselman and F. F. Lange (Plenum Press, New York, 1978) p. 667.
50. F. F. LANGE, *Int. J. Fract.* **12** (1976) 739.
51. A. G. EVANS and A. RANA, *Acta Metall.* **28** (1980) 129.

Received 25 March
and accepted 22 April 1985